ISSN 1070-3284, Russian Journal of Coordination Chemistry, 2020, Vol. 46, No. 6, pp. 430–436. © Pleiades Publishing, Ltd., 2020.

Synthesis, Structure, Photoluminescent, and Semiconductor Properties of a Novel Hg–Pr Complex

W. S. Lin[a] and W. T. Chen[a, b, *]

[a] *Department of Ecological and Resources Engineering, Fujian Key Laboratory of Eco-Industrial Green Technology, Wuyi University, Wuyishan, Fujian, 354300 P.R. China*

[b] *Institute of Applied Chemistry, Jiangxi Province Key Laboratory of Coordination Chemistry, School of Chemistry and Chemical Engineering, Jinggangshan University, Ji'an, Jiangxi, 343009 P.R. China*

**e-mail: wtchen_2000@aliyun.com*

Received August 29, 2018; revised July 3, 2019; accepted September 17, 2019

Abstract—A novel Hg-Pr compound $[Hg_3PrCl_9(HIA)(IA)_3]_n nCl \cdot 2nH_3O \cdot 4nH_2O$ (**I**) (HIA = isonicotinic acid) is prepared through the hydrothermal reactions and structurally characterized by X-ray diffraction technique (CIF file CCDC no. 1831958). This compound is characterized by a 2D organic-inorganic hybrid layer structure. Solid-state photoluminescence measurement reveals that it exhibits a photoluminescence emission in the blue region. These photoluminescence emissions correspond to the characteristic emission $^3H_4 - ^3P_J$ transitions (J = 2, 1, and 0, respectively) of Pr^{3+} ions. Solid-state UV–Vis diffuse reflectance spectrum discovers that the existence of a wide optical band gap of 3.39 eV.

Keywords: band gap, mercury, photoluminescence, praseodymium, semiconductor

DOI: 10.1134/S1070328420060044

INTRODUCTION

Lanthanide materials have recently attracted more and more attention due to their excellent photoluminescence properties [1, 2]. They show potential applications as photoluminescence emitting materials, such as electrochemical displays, light-emitting diodes (LEDs), chemical sensors, luminescence probes and so forth [3–5]. To our knowledge, lanthanide materials can exhibit strong photoluminescence emissions if the *f–f* electronic transition of the lanthanide ions can take place in high efficiency.

However, lanthanide ions generally possess a low absorption coefficient and the *f–f* electronic transition is difficult to happen. For the sake of improving the absorption coefficient and promoting the *f–f* electronic transition of the lanthanide ions to take place, scientists adopt various organic molecules which possessing a conjugated motif, for example, heterocyclic derivatives, aromatic carboxylic acids and aromatic sulfonic acids, to design and synthesize lanthanide materials. This is because these organic molecules are expected to be able to absorb the UV light and then effectively transfer the energy to the lanthanide ions, i.e. antenna effect [6–8].

Isonicotinic acid is such an organic molecule. In addition, isonicotinic acid is a very useful ligand, because it can coordinate to several metal ions. The carboxylic group of isonicotinic acid enables it to bind to lanthanide ions, while the nitrogen atom allows it to link to transition metal ions. Therefore, isonicotinic acid is an important ligand to bridge lanthanide ions and transition metal ions. Group 12 (IIB) elements are zinc, cadmium and mercury. IIB-containing compounds are attractive because of the following reasons: the wide applications of the IIB compounds, photoluminescence and photoelectric properties, the important role of zinc played in biological systems, and the various coordination numbers afforded by the d^{10} geometry of the IIB ions. We recently aim at the investigation of novel lanthanide-IIB compounds which may possess interesting photoluminescence and semiconductor properties. We report in this work the synthesis, structure, photoluminescence and semiconductor properties of a novel Hg-Pr compound $[Hg_3PrCl_9(HIA)(IA)_3]_n nCl \cdot 2nH_3O \cdot 4nH_2O$ (**I**) (HIA = isonicotinic acid), which is characterized by a 2D organic-inorganic hybrid layer structure.

EXPERIMENTAL

Materials and instrumentation. The chemicals and reagents are purchased through commercial sources and directly used. Photoluminescence experiments are carried out using the solid state powder at room temperature on a F97XP spectrometer. The UV–Vis spectra were recorded at room temperature on a computer-controlled TU1901 UV–Vis spectrometer equipped with an integrating sphere. $BaSO_4$ plate was

Table 1. Crystallographic data and structure refinement for complex **I**

Parameter	Value
Formula weight	1696.71
Color	Yellow
Crystal size, mm	0.10 × 0.08 × 0.05
Crystal system	Monoclinic
Space group	$P2_1/n$
a, Å	15.5932(8)
b, Å	9.2504(3)
c, Å	29.4734(12)
β, deg	97.360(4)
V, Å^3	4216.3(3)
Z	4
$2\theta_{max}$, deg	50
Index ranges	$-15 \le h \le 18$, $-10 \le k \le 11$, $-31 \le l \le 35$
Reflections collected	20750
Independent, observed reflections (R_{int})	5475, 6667 (0.0410)
Parameters refined	492
ρ_{calcd}, g/cm^3	2.673
μ, mm^{-1}	12.723
T, K	293(2)
F(000)	3136
R_1, wR_2	0.0679, 0.1808
Goodness-of-fit	1.022
Largest and mean Δ/σ	0 and 0
$\Delta\rho_{max}$ /$\Delta\rho_{min}$, e/Å^3	2.187/−3.710

used as a reference (100% reflectance), on which the finely ground powder of the samples was coated.

Synthesis of complex I. A mixture of $PrCl_3 \cdot 6H_2O$ (1 mmol, 376 mg), $HgCl_2$ (1 mmol, 272 mg), isonicotinic acid (2 mmol, 246 mg) and distilled water (10 mL) were sealed into a 25 mL Teflon-lined stainless-steel vessel. Then, the vessel was heated to 433 K and kept there for 10 days under autogenous pressure. When the vessel was slowly cooled down to room temperature, yellow block-like crystals were collected. The yield was 36% based on praseodymium.

For $C_{24}H_{31}Cl_{10}Hg_3N_4O_{14}Pr$			
Anal. calcd., %	C, 16.97	H, 1.82	N, 3.30
Found, %	C, 17.06	H, 1.85	N, 3.35

X-ray structure determination. A single crystal with the dimensions of 0.10 × 0.08 × 0.05 mm was carefully selected and adhered onto the tip of a glass fiber. Then the fiber was mounted to a Super Nova X-ray CCD diffractometer. The X-ray intensity data were collected by using of a graphite-monochromated MoK_α radiation (λ = 0.71073 Å) with the ω scan mode. The data set was reduced and corrected by using the Crystal-Clear software [9]. The crystal structure was solved by means of the direct solution methods and refined on F^2 by full-matrix least-squares by virtue of the Siemens SHELXTLTM V5 crystallographic software [10]. Based on the difference Fourier maps, all non-hydrogen atoms were located and refined anisotropically, while hydrogen atoms were added theoretically and not refined, but involved in the structural factor calculation with isotropic thermal parameters. Important crystallographic data are shown in Table 1, while selected bond lengths and angles are presented in Table 2.

Crystallographic data for the structural analysis have been deposited with the Cambridge Crystallographic Data Centre (CCDC no. 1831958; deposit@ccdc.cam.ac.uk or http://www.ccdc. cam.ac.uk).

Table 2. Selected bond lengths (Å) and bond angles (deg) for complex **I***

Bond	*d*, Å	Angle	ω, deg
Hg(1)–N(2)	2.160(5)	Cl(2)Hg(2)Cl(5)	79.1(5)
Hg(1)–N(4)$^{\#1}$	2.161(13)	Cl(8)Hg(3)Cl(9)	73.4(4)
Hg(1)–Cl(5)	2.779(6)	Cl(8)Hg(3)Cl(10)	136.5(3)
Hg(1)–Cl(2)	2.783(4)	Cl(9)Hg(3)Cl(10)	83.6(4)
Hg(1)–Cl(2)$^{\#1}$	3.079(3)	Cl(8)Hg(3)Cl(4)	106.0(3)
Hg(1)–Cl(4)	3.002(4)	Cl(9)Hg(3)Cl(4)	144.5(4)
Hg(2)–Cl(3)	2.304(5)	Cl(10)Hg(3)Cl(4)	113.8(3)
Hg(2)–Cl(1)	2.321(5)	Cl(8)Hg(3)Cl(7)	57.1(2)
Hg(2)–Cl(2)	2.992(5)	Cl(9)Hg(3)Cl(7)	100.4(3)
Hg(2)–Cl(5)$^{\#1}$	3.083(3)	Cl(10)Hg(3)Cl(7)	166.1(2)
Hg(3)–Cl(8)	2.291(9)	Cl(4)Hg(3)Cl(7)	55.88(19)
Hg(3)–Cl(9)	2.293(3)	Cl(8)Hg(3)Cl(5)	92.9(3)
Hg(3)–Cl(10)	2.338(8)	Cl(9)Hg(3)Cl(5)	53.6(4)
Hg(3)–Cl(4)	2.630(6)	Cl(10)Hg(3)Cl(5)	102.6(3)
Hg(3)–Cl(7)	2.656(5)	Cl(4)Hg(3)Cl(5)	91.44(19)
Hg(3)–Cl(5)	2.822(6)	Cl(7)Hg(3)Cl(5)	70.2(2)
Pr(1)–O(8)$^{\#2}$	2.392(14)	O(8)$^{\#2}$Pr(1)O(2)	74.4(5)
Pr(1)–O(2)	2.446(14)	O(8)$^{\#2}$Pr(1)O(5)	143.6(5)
Pr(1)–O(5)	2.449(12)	O(2)Pr(1)O(5)	140.3(5)
Pr(1)–O(1)$^{\#2}$	2.452(14)	O(8)$^{\#2}$Pr(1)O(1)$^{\#2}$	73.4(6)
Pr(1)–O(3)	2.458(6)	O(2)Pr(1)O(1)$^{\#2}$	116.5(5)
Pr(1)–O(7)	2.494(10)	O(5)Pr(1)O(1)$^{\#2}$	78.5(5)
Pr(1)–O(4)$^{\#3}$	2.497(11)	O(8)$^{\#2}$Pr(1)O(3)	141.8(5)
Pr(1)–O(6)$^{\#3}$	2.550(12)	O(2)Pr(1)O(3)	73.7(4)
Angle	ω, deg	O(5)Pr(1)O(3)	73.3(4)
N(2)Hg(1)N(4)$^{\#1}$	168.7(4)	O(1)$^{\#2}$Pr(1)O(3)	141.1(4)
N(2)Hg(1)Cl(5)	92.3(3)	O(8)$^{\#2}$Pr(1)O(7)	115.4(4)
N(4)$^{\#1}$Hg(1)Cl(5)	98.7(4)	O(2)Pr(1)O(7)	73.9(5)
N(2)Hg(1)Cl(2)	91.3(2)	O(5)Pr(1)O(7)	76.7(4)
N(4)$^{\#1}$Hg(1)Cl(2)	92.1(3)	O(1)$^{\#2}$Pr(1)O(7)	72.9(5)
Cl(5)Hg(1)Cl(2)$^{\#1}$	88.07(14)	O(3)Pr(1)O(7)	74.9(3)
N(2)Hg(1)Cl(4)	88.2(2)	O(8)$^{\#2}$Pr(1)O(4)$^{\#3}$	75.0(5)
N(2)Hg(1)Cl(2)$^{\#1}$	83.8(1)	O(2)Pr(1)O(4)$^{\#3}$	140.8(6)
N(4)Hg(1)Cl(4)	89.6(5)	O(5)Pr(1)O(4)$^{\#3}$	76.4(5)
N(4)Hg(1)Cl(2)	84.8(2)	O(1)$^{\#2}$Pr(1)O(4)$^{\#3}$	76.8(5)
Cl(5)Hg(1)Cl(2)	79.4(2)	O(3)Pr(1)O(4)$^{\#3}$	120.5(2)
Cl(5)Hg(1)Cl(4)	84.9(4)	O(7)Pr(1)O(4)$^{\#3}$	142.7(6)
Cl(4)Hg(1)Cl(2)	82.9(1)	O(8)$^{\#2}$Pr(1)O(6)$^{\#3}$	74.0(5)
Cl(2)Hg(1)Cl(2)$^{\#1}$	104.1(2)	O(2)Pr(1)O(6)$^{\#3}$	76.4(5)
Cl(2)Hg(1)Cl(4)$^{\#1}$	172.9(3)	O(5)Pr(1)O(6)$^{\#3}$	117.3(4)
Cl(3)Hg(2)Cl(1)	175.2(2)	O(1)$^{\#2}$Pr(1)O(6)$^{\#3}$	139.5(5)
Cl(3)Hg(2)Cl(2)	92.9(2)	O(3)Pr(1)O(6)$^{\#3}$	78.4(4)
Cl(3)Hg(2)Cl(5)	90.7(1)	O(7)Pr(1)O(6)$^{\#3}$	144.4(4)
Cl(1)Hg(2)Cl(2)	91.9(4)	O(4)$^{\#3}$Pr(1)O(6)$^{\#3}$	72.0(6)
Cl(1)Hg(2)Cl(5)	90.1(1)		

* Symmetry codes: $^{\#1}$ $-x-1/2, y+1/2, -z+1/2$; $^{\#2}$ $-x-1, -y, -z+1$; $^{\#3}$ $-x-1, -y+1, -z+1$.

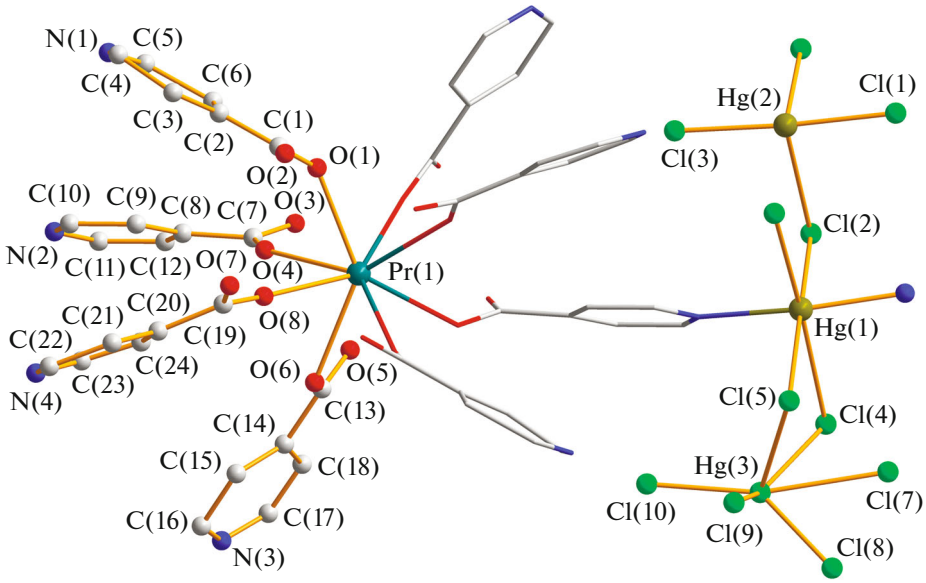

Fig. 1. The molecular structure of compound **I**. Lattice water molecules, isolated chloride ions and hydrogen atoms were omitted for clarity.

RESULTS AND DISCUSSION

The asymmetric unit of compound **I** is comprised of two praseodymium ions, two mercury ions, ten chloride anions, four isonicotinic acid ligands and six lattice water molecules, as presented in Fig. 1. The Pr(1) ion is coordinated by eight oxygen atoms from eight isonicotinic acid ligands, yielding a slightly distorted square antiprism. The top plane of the square antiprism is defined by O(5), O(3), O(6) ($-1-x$, $1-y$, $1-z$), O(4) ($-1-x$, $1-y$, $1-z$), while the bottom plane of the square antiprism is defined by O(7), O(2), O(8) ($-1-x$, $-y$, $1-z$), O(1) ($-1-x$, $-y$, $1-z$), respectively. The bond length of Pr–O locates in the expected range of 2.394(7)–2.558(6) Å with an average value of 2.470(7) Å, which is normal and comparable with those existing in the references [11–15]. The bond angles of OPrO are varied from 72.3(2)° to 144.7(2)°. Differently, the Pr(2) ion shows a distorted octahedral geometry and is surrounded by six chloride ions, of which two are μ_2-bridging and four are terminal ligands.

The Hg(1) ion displays a slightly distorted octahedral geometry, bound by four μ_2-bridging Cl atoms and two nitrogen atoms from two isonicotinic acid ligands. The Hg(2) ion is bound by two μ_2-bridging and two terminal chlorine atoms to yield a tetrahedral geometry. The Hg(3) ion is coordinated by six chlorine atoms to form a distorted octahedral geometry. The bond lengths of Hg–N are 2.160(5) and 2.161(13) Å. The bond lengths of Hg–Cl are in the region of 2.291(9)–3.083(3) Å with an average value of 2.6695(9) Å, which is normal and comparable with those documented in the references [16–20]. The bond angle of NHgN is 168.7(4)° which is close to linear. The bond angles of NHgCl are in the range of 83.8(1)°–98.7(4)° which is close to 90°. The isonicotinic acid ligands are grouped into two kinds, i.e., μ_2-bridging and μ_3-bridging ligands. The μ_2-bridging isonicotinic acid ligands link two neighboring praseodymium ions with two oxygen atoms of the carboxylic group. The μ_3-bridging isonicotinic acid ligands bridge two neighboring praseodymium ions with two oxygen atoms of the carboxylic group and coordinate to one mercury ion with the nitrogen atom of the pyridyl ring. The pyridyl rings of the isonicotinic acids are almost coplanar with the deviation of the atoms on the pyridyl ring in a narrow span of –0.077...+0.074 Å apart from their average ring plane.

Every two neighbouring praseodymium ions are interlinked by four isonicotinic acid ligands to yield a one-dimensional (1D) $-Pr-(IA)_4-Pr-(IA)_4-$ chain, as shown in Fig. 2a. The distances between neighbouring praseodymium ions are 4.5795(5) and 4.7368(5) Å. There is another kind of 1D chain existing in complex **I**. The mercury ions are interconnected by the bridging chloride ions, yielding a 1D chain, as shown in Fig. 2b. These two kinds of 1D chains are further interconnected by the isonicotinic acid ligands, forming a two-dimensional (2D) organic-inorganic hybrid layer, as shown in Fig. 3.

In complex **I**, there are several N–H···O, C–H···O, and C–H···Cl hydrogen-bonding interactions (i.e. N(3)–H(3*B*)···O(5*w*) 2.72(2) ($-2-x$, $1-y$, $1-z$), 152; C(16)–H(16*A*)···O(6*w*) ($-1/2-x$, $1/2+y$, $1/2-z$) 3.377(17), 152; C(18)–H(18*A*)···O(1) ($-1-x$, $-y$, $1-z$) 3.477(14), 169; C(22)–H(22*A*)···Cl(3) ($-1/2-x$, $1/2+y$, $1/2-z$) 3.557(9), 137; C(23)–

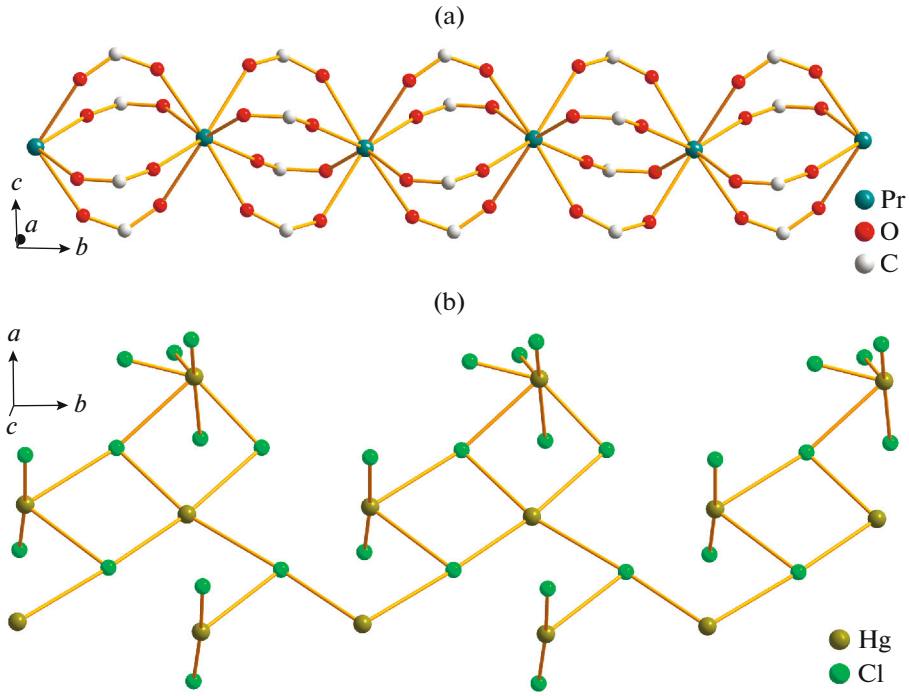

Fig. 2. Two types of 1D chains existing in compound **I**: a 1D $-Pr-(IA)_4-Pr-(IA)_4-$ chain (a); a 1D Hg–Cl chain (b).

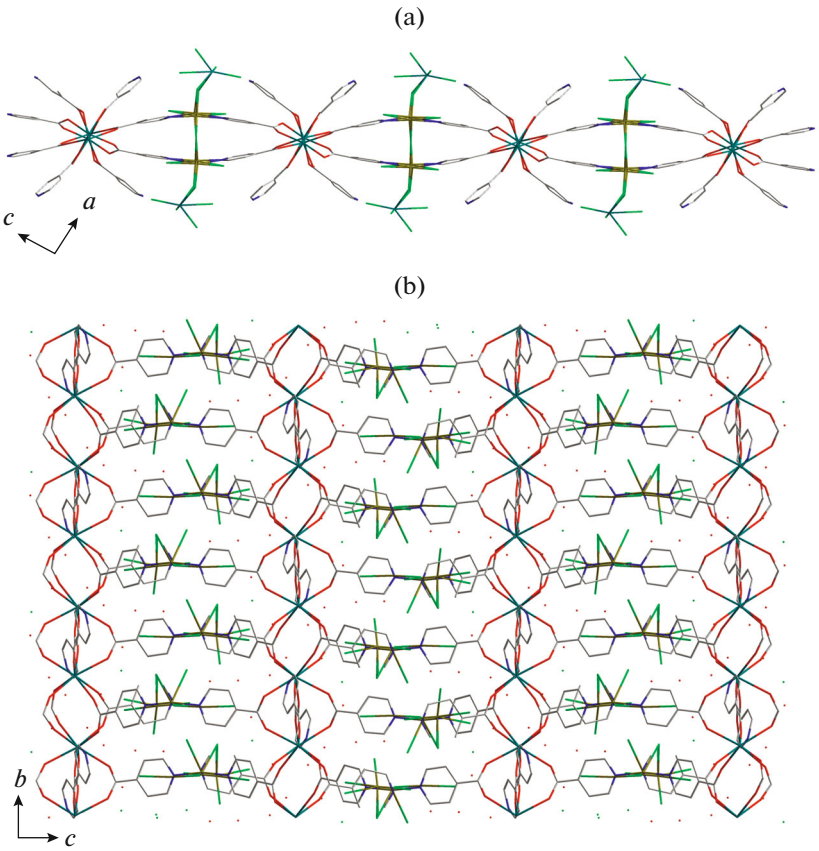

Fig. 3. The 2D layer of compound **I** viewed from different directions.

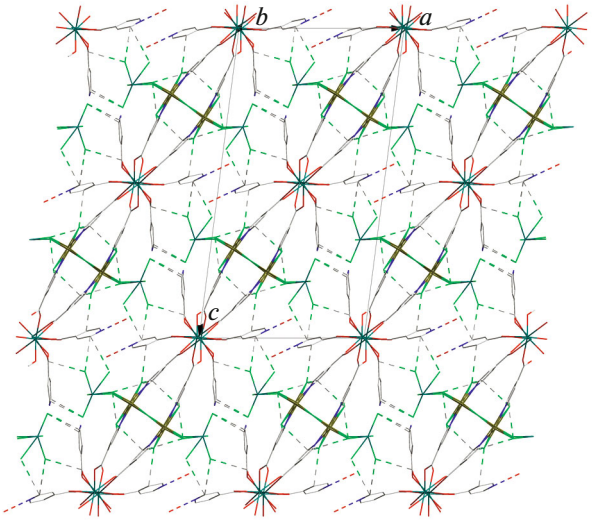

Fig. 4. The packing diagram of compound **I** with the dashed lines representing hydrogen bonding interactions.

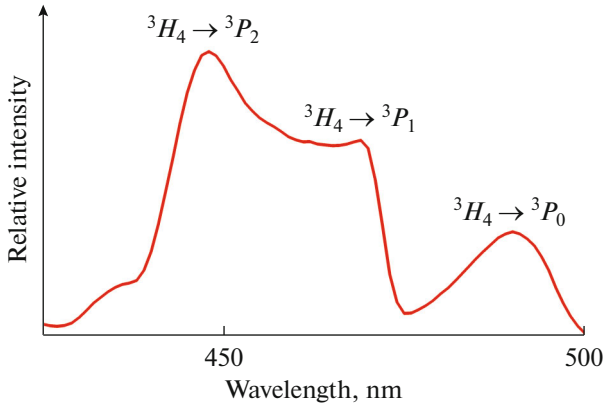

Fig. 5. The solid-state photoluminescence spectra of **I** (λ_{ex} = 275 nm).

H(23*A*)···Cl(3) (−1/2 − *x*, −1/2 + *y*, 1/2 − *z*) 3.674(9), 157). These hydrogen-bonding interactions are important, because they connect the 2D layers together to yield a 3D supramolecular network, as presented in Fig. 4. To the best of our knowledge, complex **I** is the first example of praseodymium-mercury isonicotinic acid complexes with isonicotinic acid bridging praseodymium and mercury ions, although some praseodymium isonicotinic acid complexes [21, 22] or mercury isonicotinic acid complexes [23–25] have been documented so far.

To our knowledge, lanthanide complexes can generally show photoluminescence properties and a lot of investigations in this field have been carried out. Complex **I** is expected to display good photoluminescence properties. In this work, the photoluminescence performance of complex **I** was carried out by using solid state samples at room temperature. The result of the photoluminescence measurements is presented in Fig. 5. It can be found that the photoluminescence spectrum of complex **I** shows an effective energy absorption in the wavelength region of 260–320 nm. The excitation spectrum of complex **I** has one maximum peak at 296 nm, when it was excited by 448 nm. We then measured the corresponding photoluminescence emission spectrum of complex **I**, upon irradiation with the wavelength of 296 nm. The emission spectrum is characteristic of a wide band in the range of 430–500 nm with three peaks locating at 448, 469, and 490 nm, respectively. These sharp peaks correspond to the characteristic emission $^3H_4$–^3P_J transitions (J = 2, 1, and 0, respectively) of Pr^{3+} ions [26, 27]. This indicates that effective energy transfer takes place and a conjugated system is formed between the isonicotinic acid ligands and the Pr^{3+} ions. So, isonicotinic acid is a good antenna for the title complex. These emission bands locate in the blue region of the light spectrum. As a result, complex **I** can be a candidate of potential blue light photoluminescent materials.

The absorption spectra of complex **I** were measured from the solid-state UV–Vis diffuse reflectance spectra with the Kubelka–Munk function, i.e., $\alpha/S = (1 - R)^2/2R$. The α in this function is the absorption coefficient, S means the scattering coefficient that is practically wavelength independent when the particle size is larger than 5 μm, while R means the reflectance. The value of the optical band gap can be determined by extrapolating from the linear portion of the absorption edge from the α/S vs. energy gap (E_g) plot. As depicted in Fig. 6, the solid-state diffuse reflectance spectra reveal that complex **I** displays a wide optical band gap of 3.39 eV. As a result, complex **I** is a candidate for wide band gap semiconductor materials. The gentle slope of the optical absorption edge of complex **I** suggests that it is an indirect transition [28]. The optical band gap of 3.39 eV of complex **I** is smaller than that of diamond (5.47 eV) which is one of the third generation semiconductor materials, but is obviously larger than that of GaAs (1.42 eV), CdTe (1.5 eV) and $CuInS_2$ (1.55 eV), all of the later are efficient photovoltaic materials [29, 30]. The optical absorption of complex **I** is probably originated from the charge-transfer excitations mainly from the *p*-like valence band of the chloride ions to the 4*f*-like conduction band of the mercury ions. There are several small peaks residing at between 2.0 and 3.0 eV which is probably ascribed to the Pr^{3+} ions.

In brief, a praseodymium material is prepared through the hydrothermal reactions and structurally characterized by X-ray diffraction technique. The title complex is characterized by a 2D organic-inorganic hybrid layer structure. The hydrogen-bonding interactions connect these 2D layers together to yield a 3D supramolecular network. Solid-state photoluminescence measurement reveals that it exhibits an emission

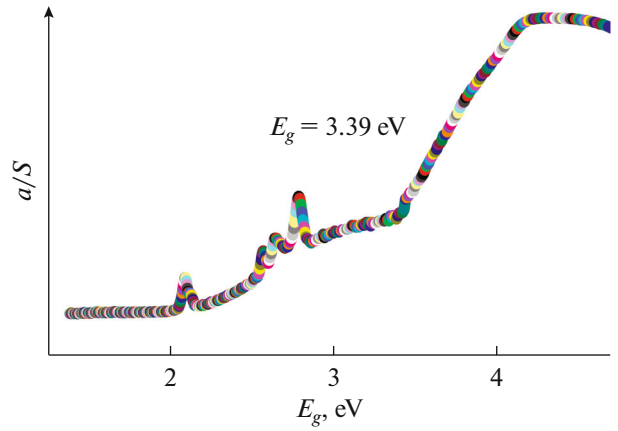

Fig. 6. Solid-state diffuse reflectance spectrum of **I**.

in the blue region. It can be used as a blue light emitting material. Solid-state UV–Vis diffuse reflectance spectrum discovers that the existence of a wide optical band gap of 3.39 eV, suggesting that it is potentially a wide band gap semiconductor.

FUNDING

We thank the financial support of the NSF of China (nos. 21361013, 31460488), NSF of Fujian (no. 2018J01447), Jiangxi Provincial Department of Education's Item of Science and Technology (GJJ170637), and the open foundation (no. 20180008) of the State Key Laboratory of Structural Chemistry, Fujian Institute of Research on the Structure of Matter, Chinese Academy of Sciences.

REFERENCES

1. Zhang, Q.Q., Wu, L.L., Cao, X.Y., et al., *Angew. Chem. Int. Ed.*, 2017, vol. 56, p. 7986.
2. Ban, R., Sun, X.P., Wang, J.W., et al., *Dalton Trans.*, 2017, vol. 46, p. 5856.
3. Wan, Y., Sun, W., Liu, J., et al., *Inorg. Chem. Commun.*, 2017, vol. 80, p. 53.
4. Zhou, W., Gu, M., Ou, Y., et al., *Inorg. Chem.*, 2017, vol. 56, p. 7433.
5. Guo, H., Zhu, S., Cai, D., et al., *Inorg. Chem. Commun.*, 2014, vol. 41, p. 29.
6. Coban, M.B., Amjad, A., Aygun, M., et al., *Inorg. Chim. Acta*, 2017, vol. 455, p. 25.
7. Rong, J.W., Zhang, W.W., and Bai, J.F., *Rsc. Adv.*, 2016, vol. 6, p. 103714.
8. Matthes, P.R., Eyley, J., Klein, J.H., et al., *Eur. J. Inorg. Chem.*, 2015, vol. 5, p. 826.
9. Rigaku, Crystal Clear, Version 1.35, Tokyo: Rigaku Corporation, 2002.
10. Siemens, SHELXTL^{TM}, Version 5, Madison: Reference Manual, Siemens Energy & Automation Inc., 1994.
11. Li, Q., Chen, S., Yan, P., et al., *J. Coord. Chem.*, 2013, vol. 66, p. 1084.
12. Zhao, F.-H., Liang, S.-H., Jing, S., et al., *Inorg. Chem. Commun.*, 2012, vol. 21, p. 109.
13. Zhuang, G., Chen, W., Zheng, J., et al., *J. Solid State Chem.*, 2012, vol. 192, p. 284.
14. Wang, C., Wang, Y., Qin, Z., et al., *Inorg. Chem. Commun.*, 2012, vol. 20, p. 112.
15. Zhang, J., Huang, J., Yang, J., et al., *Inorg. Chem. Commun.*, 2012, vol. 17, p. 163.
16. Dolai, M., Mistri, T., Panja, A., et al., *Inorg. Chim. Acta*, 2013, vol. 399, p. 95.
17. Zhu, H.-B., Yang, W.-N., and Shan, R.-Y., *J. Chem. Res.*, 2012, vol. 36, p. 598.
18. Paqhaleh, D.S., Hashemi, L., Amani, V., et al., *Inorg. Chim. Acta*, 2013, vol. 407, p. 1.
19. Ni, J., Pan, Y.-Z., Wei, Z.-R., et al., *Inorg. Chem. Commun.*, 2013, vol. 30, p. 17.
20. Kumar, G. and Gupta, R., *Inorg. Chem. Commun.*, 2012, vol. 23, p. 103.
21. Li, X., Huang, Y., and Cao, R., *Cryst. Growth Des.*, 2012, vol. 12, p. 3549.
22. Chen, H.-M., Hu, R.-X., and Zhang, M.-B., *Inorg. Chim. Acta*, 2011, vol. 379, p. 34.
23. Liu, D.-S., Chen, W.-T., Huang, J.-G., et al., *CrystEngComm*, 2016, vol. 18, p. 7865.
24. Machura, B., Switlicka, A., Zwolinski, P., et al., *J. Solid State Chem.*, 2013, vol. 197, p. 218.
25. Chen, W., Hu, L., Lai, C., et al., *J. Chem. Res.*, 2010, vol. 34, p. 533.
26. Lakshminarayana, G. and Qiu, J., *Phys. B* (Amsterdam, Neth.), 2009, vol. 404, p. 1169.
27. Lakshminarayana, G., Qiu, J., Brik, M.G., et al., *J. Phys., D*, 2008, vol. 41, p. 175106.
28. Huang, F.Q., Mitchell, K., and Ibers, J.A., *Inorg. Chem.*, 2001, vol. 40, p. 5123.
29. Tillinski, R., Rumpf, C., Nather, C., et al., *Z. Anorg. Allg. Chem.*, 1998, vol. 624, p. 1285.
30. Dürichen, P. and Bensch, W., *Eur. J. Solid State Inorg. Chem.*, 1997, vol. 34, p. 1187.